IEEE Access
Multidisciplinary | Rapid Review | Open Access Journal

Received 18 September 2022, accepted 7 October 2022, date of publication 10 October 2022, date of current version 19 October 2022.

Digital Object Identifier 10.1109/ACCESS.2022.3213685

RESEARCH ARTICLE

Investigation of Single-Event-Transient Effects Induced by Heavy-Ion in All-Silicon DG-TFET

ASHISH MAURYA[1], KALYAN KOLEY[2], (Senior Member, IEEE), JITENDRA KUMAR[1], (Senior Member, IEEE), AND PANKAJ KUMAR[1], (Graduate Student Member, IEEE)

[1]Indian Institute of Technology, Dhanbad, Dhanbad, Jharkhand 826004, India
[2]Birla Institute of Technology, Mesra, Ranchi, Jharkhand 835215, India

Corresponding author: Ashish Maurya (er.ashish.maurya91@gmail.com)

ABSTRACT The heavy-ion analysis is a single-event-effect (SEE) that produces a single-event-transient (SET) pulse of current. In this work, the analysis was done to observe the maximum impact of heavy-ions on a calibrated double-gate tunnel field-effect transistor (DG-TFET) taken as a device under test (DUT). The impact of heavy-ions on DG-TFET is compared with the previous work done for different TFETs. The ions are directed to strike vertically at five different positions; source, source-body junction, body, drain-body junction, and the drain region of DG-TFET. The analysis is done by observing the heavy-ion generation rate, heavy-ion charge density, and transient current for the strike of the ion at different locations on the DUT and at different linear energy transfer (LET) values with the help of physics-based numerical simulation. In the study, a detailed analysis of the transient current due to a heavy-ion strike in the body region is reported, and this transient current is compared with the existing reported data for different FETs. Bipolar gain of the device is also observed for a heavy-ion strike in the body region, which is an important parameter for analyzing SEE. The findings in this study can give a new insight into SEE in TFET devices and can also provide guidelines for radiation-hardened applications for TFET-based circuits.

INDEX TERMS Tunnel FET, heavy-ion irradiation, single-event-effects, transient analysis, bipolar gain.

I. INTRODUCTION

Switching is a key feature of field-effect transistors (FETs) and, because of having a better switching speed than bipolar transistors, metal-oxide-semiconductor (MOS) technology has ruled over the semiconductor industry for many decades. Metal-oxide-semiconductor FETs (MOSFETs) were a revolution for the semiconductor industry, as now many low-power applications are based on this. However, the era of MOSFET is tending to an end as the technology moves towards the nanoscale from the microscale. Thus, the search for a new device that extends low-power circuit applications further is on. Tunnel FET (TFET) is a device that can replace the MOSFET because it has the advantage of overcoming the issue of short-channel effects (SCEs) occurring in the MOSFETs [1], [2], [3], [4], [5], [6].

The associate editor coordinating the review of this manuscript and approving it for publication was Ye Zhou.

Due to the band-to-band tunneling (BTBT) mechanism, TFET achieves subthreshold-swing (SS) below 60 mV/dec and low subthreshold leakage current, which makes it a promising candidate for low-power applications [5], [6], [7]. TFET has a high ON-current to OFF-current ratio as well, which makes it highly recommendable for low-power applications and suitable for space electronics [8].

Semiconductor industries working on space electronics have a big concern of radiation in space. Radiation induces soft errors in the devices, which impacts the reliability of integrated circuits [9], [10]. Among different radiations, heavy-ion irradiation is found more in the space where artificial satellites are placed [9]. Heavy-ion irradiation is a single-event effect (SEE) that causes soft errors in the device. A heavy-ion loses energy and generates a stream of electron-hole pairs when it penetrates a device. The generated additional electrons and holes cause an instant large current to switch the logic state of a device [11].

The impact of heavy-ion irradiation is analyzed in various FETs through various parameters in [12], [13], [14], [15], [16], [17], and [18]. In [12], the simulation study was done to analyze the sensitivity of the fully depleted SOI-MOSFET. The study shows that with the increase in heavy-ion energy, the bipolar gain of the transistor decreases; this analysis is done through the calculation of collected charge during and after the incident of heavy-ions. In [13], various radiation sources and their mechanisms are discussed. It is found that SEE is an instantaneous effect and can cause a large impact on the device. The impact of heavy-ions on SOI devices is also observed in [14] and [15] by calculating drain collected charges. The study is done through transient response for SEE in SOI like bulk MOSFET [16] and in Si-nanowire FET [17]. In [17], the considered device heavy-ion incident is taken at the channel/drain junction, and the detrimental impact is observed on CMOS inverter characteristics. In [18], the single event of multiple transient structures is proposed to analyze the impact of heavy-ions, and their result shows that the charge sharing can impact three transistors at most.

It is observed that the collected charge is one of the most important parameters to analyze the impact of heavy-ions on the devices under test (DUT). In this work, the focus has been put on the collected charge and the transient current of the DUT. As the TFET emerges as a promising candidate for low-power electronics and by over serving the immense impact of heavy-ions on space electronics, the impact of heavy-ions on various characteristics of the TFET is conducted by transient simulation in the Sentaurus TCAD tool [11]. In [19] and [20], the studies are done on an effective ion-track model as the energy deposition and e-h pair generation happen around the track. The three different ways to model the ion track are discussed, in which the event-by-event approach is found to be more accurate than the other approaches. However, the focus is given to increasing the accuracy of the average approach by defining ion-track dependency on the radial distance parameters. With the shrinking size of devices, the calculation of the spatial and temporal track structure of an ion has become important [21]. In the Sentaurus heavy-ion model, both the track structures are considered.

Sentaurus heavy-ion model has a radial distribution of energy in its heavy-ion physics model and it is defined by defining the spatial distribution in the physics of the heavy-ion model [11], [28]. The analysis also includes total charge density and instant generation rate caused by heavy-ions, known as heavy-ion charge density and heavy-ion generation rate, to analyze the heavy-ion effects. First, the analysis is carried out to find the most sensitive region in the device against heavy ions by striking the heavy-ion at different locations of the DUT, and thereafter the detailed analysis is done for the most sensitive region for different linear energy transfer (LET).

Key points of this work are-

1. Heavy-ion impact is analyzed by using a physics-based numerical simulation model of Sentaurus TCAD.
2. All the possible sensitive locations have been observed for the analysis of the impact of heavy-ion.
3. Among all the locations, the body region is found to be the most sensitive and so the detailed analysis is done for the strike of heavy-ion at different LETs.
4. Maximum observed transient current for different LETs and the corresponding collected charge is discussed in the report.
5. Bipolar gain is calculated for different LETs when heavy-ion strikes at the body region.

II. DEVICE DESCRIPTION AND HEAVY-ION SIMULATION METHODOLOGY

A. DEVICE DESCRIPTION AND VALIDATION

To analyze the impact of heavy-ions in TFETs, all-silicon double-gate nTFET (DG-nTFET) is taken as a DUT. To validate the DUT of this work, a 2 μm gate length TFET model is used from [22], and the calibrated graph is shown in Fig. 1(b). The TFET model of 2 μm is considerable because the tunneling current is independent of the gate length [23], [24], it depends on tunneling width. The device has achieved 0.05 μA/μm ON-current at $V_d = 0.6\ V$ at 300 K. The

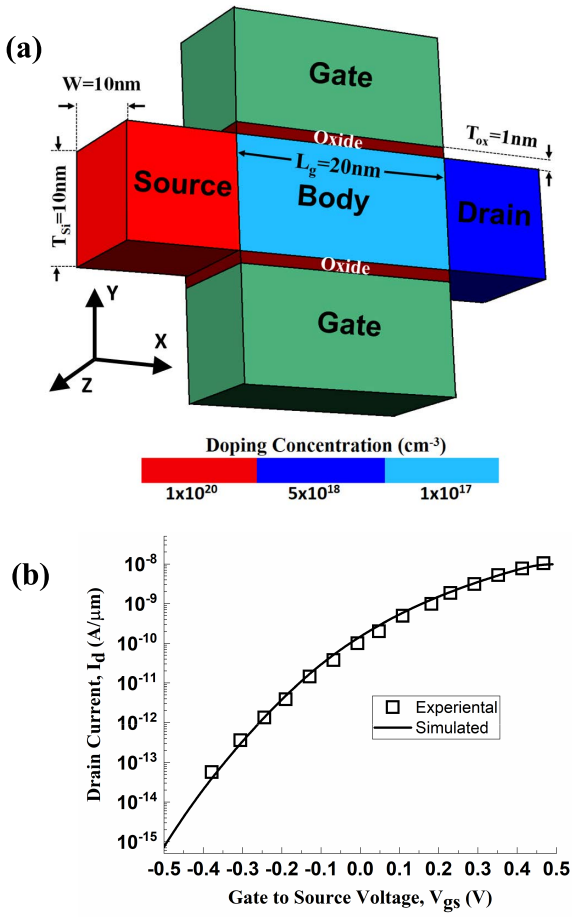

FIGURE 1. (a) 3-D schematic of the simulated Si DG-nTFET device, and (b) Comparison of transfer characteristics of simulated and experimental TFET at $V_d = 0.6$ V.

physical parameters of the DUT are: gate length (L_g) = 20 nm; effective oxide thickness (EOT) = 1 nm; and channel thickness (T_{Si}) = 10 nm. The structure of DG-nTFET is shown in Fig. 1(a). The doping in the regions are, Drain doping (n-type) = 5×10^{18} cm^{-3}; Source doping (p-type) = 1×10^{20} cm^{-3}; Channel doping (n-type) = 1×10^{17} cm^{-3}. The source, channel, and drain regions are uniformly doped. In the calibrated model, the reduced tunneling mass (m_r) is used as a fitting parameter to get the prefactor (A_{path}) and exponential factor (B_{path}) for generation rate in non-local BTBT. Molybdenum (workfunction = 4.53 eV) is used as a gate metal.

As the generation and recombination parameters govern the characteristics and performance of the device, 3-D device simulations are performed with two recombination models: the Shockley-Read-Hall (SRH) recombination model and the Auger recombination model. The Auger recombination model is used to model the loosely bound electron-hole pairs at lower carrier densities. The Philips unified mobility model proposed by Klaassen is used in this study. The Philips mobility model unifies the description of screening of ionized impurities by charge carriers, electron-hole scattering, majority and minority carrier bulk mobilities, and temperature dependency. To account the high doping concentration, the Fermi-Dirac statistic model is used along with the high-field velocity saturation and the bandgap-narrowing models of Sentaurus TCAD [11]. The tunneling current is estimated using Kane's BTBT generation model [5], which is given by the equation:

$$I_d \approx T_P \approx A_{path} \exp\left(-B_{path} W_t^{1.5}\right) \tag{1}$$

where, I_d is the drain current, T_P is tunneling probability, A_{path} and B_{path} are Kane's pre and exponential factors, respectively. W_t is tunneling barrier width which controls the ON-current. Kane's BTBT generation model [11] is defined by-

$$G_r = A_{path} \left(\frac{E}{E_0}\right)^P \exp\left(-\frac{B_{path}}{E}\right) \tag{2}$$

where, $E_0 = 1$ V/cm; $P = 2.5$; for indirect BTBT. E is the electric field.

$$A_{path} = \frac{g\,(m_c m_v)^{\frac{3}{2}}\,(1 + 2N_{TA})\,D_{TA}^2\,(qF_0)^{\frac{5}{2}}}{2^{\frac{21}{4}} h^{\frac{5}{2}} m_r^{\frac{5}{4}} \rho \varepsilon_{TA} E_g^{\frac{7}{4}}} \tag{3}$$

$$B_{path} = \frac{2^{\frac{7}{2}} \pi m_r^{\frac{1}{2}} E_g^{\frac{3}{2}}}{3qh} \tag{4}$$

where, N_{TA}, D_{TA} and ε_{TA} are the occupation number, deformation potential and the energy of the transverse acoustic phonon, respectively; ρ is the mass density; $m_c(m_v)$ is the CB (VB) density of states effective mass; q is the elementary charge; h is Planck's constant; g is a degeneracy factor; m_r is the reduced tunneling mass, and E_g is the minimum bandgap.

B. HEAVY-ION SIMULATION

The process flow of the heavy-ion simulation study is shown in the flow graph in Fig. 2. The DUT is taken for the study

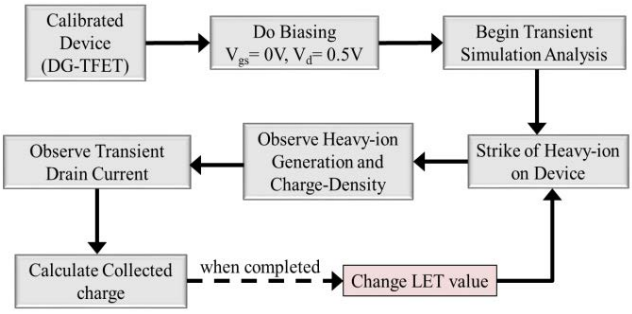

FIGURE 2. Process flow of simulation study of impact of heavy-ion in DG-nTFET.

is DG-nTFET, shown in Fig. 1(a), the device is well calibrated with [22] and the meshing strategy follows [25] for the precision in the analysis. As the radiation is known for switching the device from OFF-state to ON-state, the next step of the process device is biased in the OFF-state. In the biasing strategy, drain voltage (V_d) is taken to 0.5 V and gate-to-source voltage (V_{gs}) is set to zero along with the body. The transient analysis is carried out in this work due to the impact of heavy-ion radiation being dependent on the time of the incident and the time that heavy-ions take to cross the device. The next step in the simulation study is the strike of heavy ion at different positions in the device and finding the most sensitive position against heavy ions.

This work is analyzing the impact of heavy-ion strikes on DG-TFET for maximum impact. In Table 1, max I_d and Q_C are shown with the TFETs from the published data in [5], [15], [26], [27] and [36] for DUTs in the OFF-state at $V_{gs} = 0$ V. All the TFETs taken for heavy-ion impact analysis have a 0.5 V drain voltage except for the TFET of literature [27] which has a V_{ds} of 1.5 V. The LET of heavy-ions which strike on tabulated DUTs is 10 MeV-cm^2/mg. It shows that the DUT of this work has the maximum impact on heavy-ions compared to the tabulated TFETs. Maximum collected charge means heavy-ion creating a greater number of electron-hole pairs in the device and rise in the potential; due to this the SET immunity also decreases.

TABLE 1. Observed maximum transient drain current and collected charge for DUTs from previous works [5], [15], [23], and [24] and this work when heavy-ion strikes at LET = 10 MeV-cm^2/mg for devices in OFF-state.

	DUT	Max I_d (μA)	Max Q_C (fC)
Suman Datta (MR 2014) [5]	HTFET	56	-
Qianqiong Wang (TNS 2018) [15]	LTFET	260	2.1
Guoliang Tian (SST 2020) [26]	DG-FeTFET	272	2
Y. Wu (232nd ECS Meeting 2017) [27]	Conventional TFET	1600	52
M. Sharma (VLSIDCS 2022) [36]	Dopingless TFET	453	2.92
This Work	DG-TFET	103	538

While defining the heavy-ion model, the compatibility of ion-track radius and the corresponding LET values should be verified and also the radius should be defined in such a way that it would cover the sensitive area/location of the device. Hence, in this study, the physics of the heavy-ion incident is incorporated into the device through the heavy-ion model of Sentaurus TCAD [11] in such a way that it would have properties close to real heavy-ions. The position of the strike of heavy-ions is shown by arrows in Fig. 3. A total of 5 different positions of the heavy-ion strike have been taken in this report; source region, source-body junction, body region, drain-body junction, and drain region. The ions are directed to strike vertically at x-coordinates; 5, 10, 20, 30, and 35 nm as shown in Fig. 3. 3-D device simulations are performed for the analysis of the impact of heavy-ions, and the meshing in the device is designed in such a way that the mesh spacing is small compared to the width of the ion-track to ensure accurate generation.

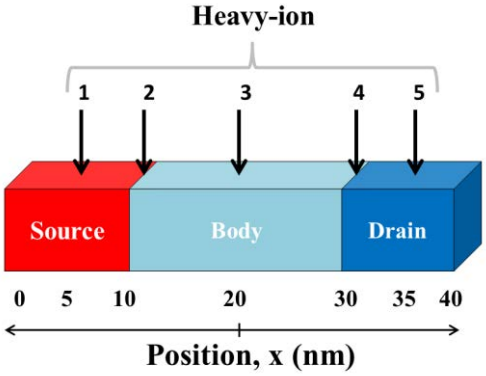

FIGURE 3. The x-coordinates of different heavy-ion tracks considered in the simulations.

The analysis of the impact of heavy-ions is done through heavy-ion carrier generation in the device and the heavy-ion charge density, which is the next step. The ion-generation rate (Gr_{ion}) in the device is caused by a heavy-ion strike and is calculated by the mathematical expression [11], [28]:

$$G_{r_{ion}}(l, r, t) = G_{rLET}(l) \quad R_{ion}(r, l) \quad T_{ion}(t) \tag{5}$$

where, Gr_{LET} is the linear energy transfer generation density in pairs/cm^3 and its simplified equation is given in (6) by considering the default values of coefficients for carrier generation [11]. R_{ion} and T_{ion} are functions for spatial and temporal distributions of the generation rate respectively. The distribution of heavy-ion carrier generation is taken to be Gaussian in this study. So, the spatial and temporal distributions are defined by the Gaussian function as given in (7) and (8).

$$G_{rLET} = \frac{1}{\pi r_0^2} LET\_f(l) \tag{6}$$

$$R_{ion}(r, l) = \exp\left(-\left(\frac{r}{r_0}\right)^2\right) \tag{7}$$

$$T_{ion}(t) = \frac{2\exp\left(-\left(\frac{t-t_0}{\sqrt{2}w_0}\right)^2\right)}{\sqrt{2}w_0\sqrt{\pi}\left(1 + erf\left(\frac{t_0}{\sqrt{2}w_0}\right)\right)} \tag{8}$$

LET_f is defined in pC/μm in the heavy-ion model by mentioning the keyword PicoCoulomb in the physics section. The variable r is the perpendicular radius distance from the ion track and the variable t is the time, while r_0 and w_0 are the characteristic values of the Gaussian function. The ion strike is modeled using Gaussian radial distribution with 10 nm characteristics radius [17], Gaussian time distribution is set to center at 20 ps with characteristics width of 2 ps [15], [31].

The next step is the observation of transient drain current; the transition of e-h pairs in the sensitive volume of the device forms the transient current pulse. This pulse of current is also known as a single-event transient (SET) pulse. The final analysis is done by calculating the collected charge on the device. The collected charge is obtained by the integration of simulated transient drain current over transient time, given in (9).

$$Q_C = \int_0^t I_d dt \tag{9}$$

Q_c is the collected charge in the device and I_d is the transient drain current.

From the step of ion-strike, the process is repeated for six different LET values; LET = 1, 4, 7, 10, 14, and 20 MeV-cm^2/mg, which are considered for the worst case scenario following [21], [32], [33], [34], [35], and for which the results are analyzed and discussed in the next section.

III. RESULTS AND DISCUSSION

A. ION STRIKES AT DIFFERENT POSITIONS

In this section, we have first analyzed the impact of heavy-ions at different positions for the highest LET (i.e. 20 MeV-cm^2/mg), and then the analysis is done for the position at which transient impact is most sensitive. Ion strikes at different positions are considered between the source (x = 0 nm) and the drain (x = 40 nm), as shown in Fig. 3.

The Gaussian distribution of heavy-ion generation in the device is shown by the x-z cross-sectional view in Fig. 4(a), (b), (c), (d), and (e) at all the positions for LET = 20 MeV-cm^2/mg. It can be seen in the cross-sectional figures of Fig. 4 that the ion generation is maximum at the position where an ion strikes, and after that, it follows a Gaussian distribution. The maximum ion generation when ion strikes in the source and drain regions is of a lower value of order 10^{32} cm^{-3}sec^{-1}, and for the other positions, it is of the higher value of order 10^{32} cm^{-3}sec^{-1}, the highest for the body region. Due to the heavy-ion strike and the ion generation, charge density in the device also varies and justifies the heavy-ion generation rate. As the variation in charge density is caused by heavy-ions, so it is called heavy-ion charge density. The variation in the heavy-ion charge density is shown in Fig. 5, this also follows Gaussian distribution

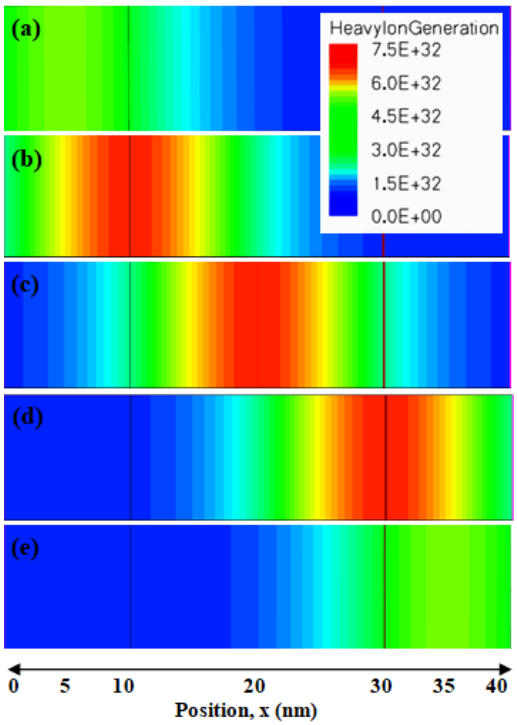

FIGURE 4. Showing x-z cross-sectional view of the device for heavy-ion generation rate at different positions for LET = 20 MeV-cm^2/mg; (a) source region, (b) source-body junction, (c) body region, (d) drain-body junction, and (e) drain.

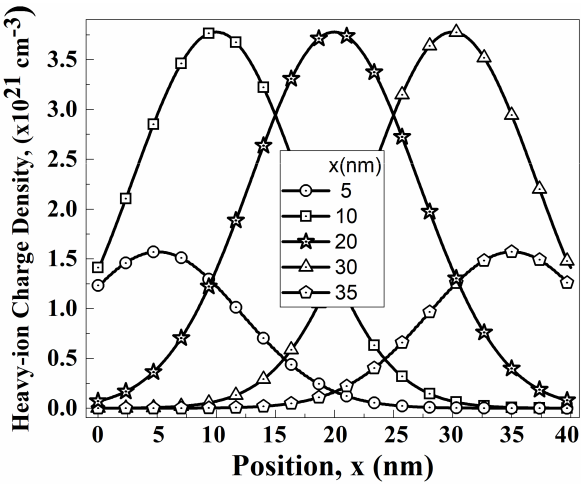

FIGURE 5. The variation in the heavy-ion charge density is shown with respect to position for ion strikes at different positions at LET = 20 MeV-cm^2/mg.

same as heavy-ion generation and achieved the peak at the position where ion strikes.

Ionized e-h pairs are collected along the ion track when a heavy-ion strikes and passes through the sensitive volume of the device. And when this collected charge exceeds the critical charge, the logic state of the device changes from OFF-state to ON-state. Figure 6 shows the pulses of transient current for different positions of ion-strike at

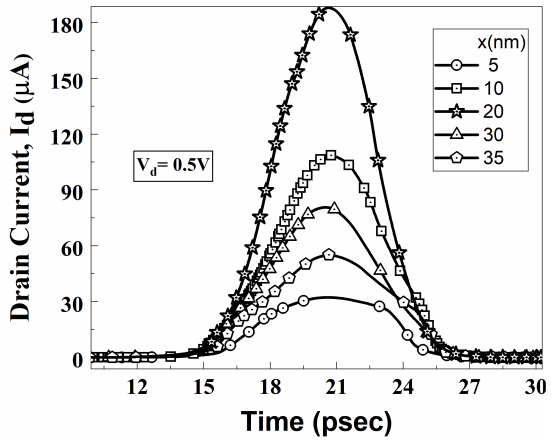

FIGURE 6. The variation in the transient drain current is shown for different positions at LET = 20 MeV-cm^2/mg with respect to time at 0.5 V drain voltage.

LET = 20 MeV-cm^2/mg. The analysis is done for 0.5 V drain voltage (V_d) and zero gate-to-source voltage (V_{gs}), the device with this biasing works in the OFF-state. The observed spike in the drain current is for around 12ps and the peak is achieved at 20ps when an ion penetrates the device. The maximum drain current is observed for position x = 20 nm when the ion strikes the body region, and it is approximately 188 μA. The minimum drain current is observed for position x = 5 nm, for the source region. Similar to the observed drain current, the maximum charge is collected when the ion strike at position x = 20 nm and the minimum charge at position x = 5 nm. The collected charge is calculated by (8), and the graph is shown in Fig. 7.

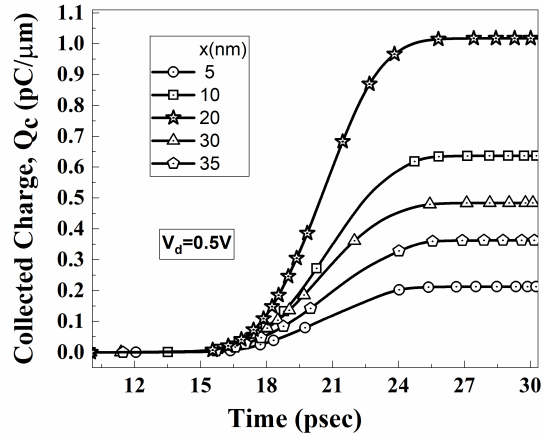

FIGURE 7. The collected charge in the device is shown for different positions with respect to time at LET = 20 MeV-cm^2/mg.

It is observed from the drain current graph that the body is the most sensitive to the heavy-ion for LET = 20 MeV-cm^2/mg. So, further, it becomes important to analyze the variation in the drain current for different LETs at different positions, as shown in Fig. 8. The marked area with a circle in Fig. 8 shows the drain current for an ion strike

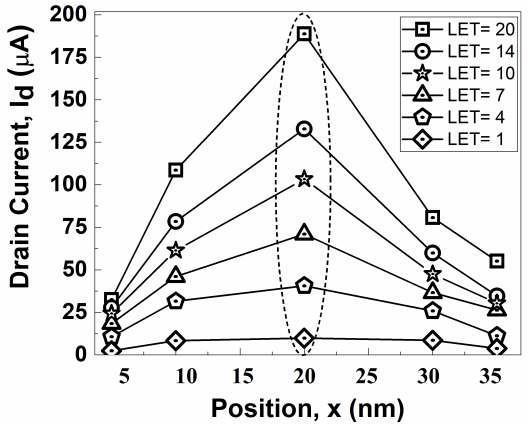

FIGURE 8. Variation in maximum drain current for different LETs when heavy-ion strikes at different location at DG-TFET.

at the body region, and it is observed that the increment in drain current with an increase in LET is greater for position x = 20 nm as compared to the other positions. So further, in this report, the analysis and discussion are done for ion strike at the body region at different LETs through heavy-ion generation, charge density, transient drain current, collected charge, and the bipolar gain.

B. SENSITIVITY WHEN ION STRIKES AT BODY REGION

The Gaussian distribution of heavy-ion generation in the device is shown by the x-z cross-sectional view of the investigated device in Fig. 9 for different LETs. The variation in the ion-generation for LET = 1, 4, 7, 10, 14, and 20 MeV-cm^2/mg is shown in Fig. 9(a), (b), (c), (d), (e), and (f), respectively. It can be seen in the cross-sectional figures of Fig. 9 that the ion generation is maximum at the position where the ion strikes, similar to the previous discussion made for Fig. 4. The variation in the heavy-ion charge density is shown in Fig. 10, this also follows a Gaussian distribution, which it should be, and the peak is at the center of the body region.

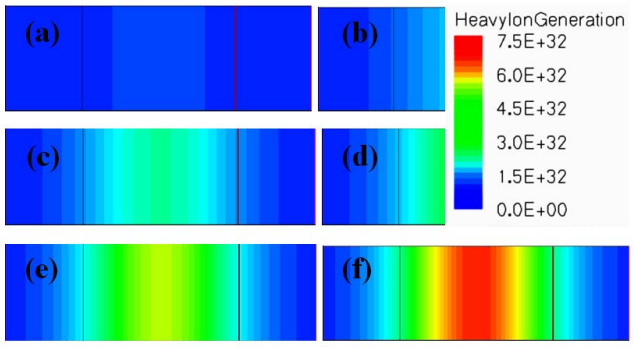

FIGURE 9. Showing x-z cross-sectional view of the device for heavy-ion generation at different LETs (MeV-cm^2/mg); (a) 1, (b) 4, (c) 7, (d) 10, (e) 14 and (f) 20.

In Fig. 11, the variation in the potential of the device due to heavy-ions is observed for different LET values.

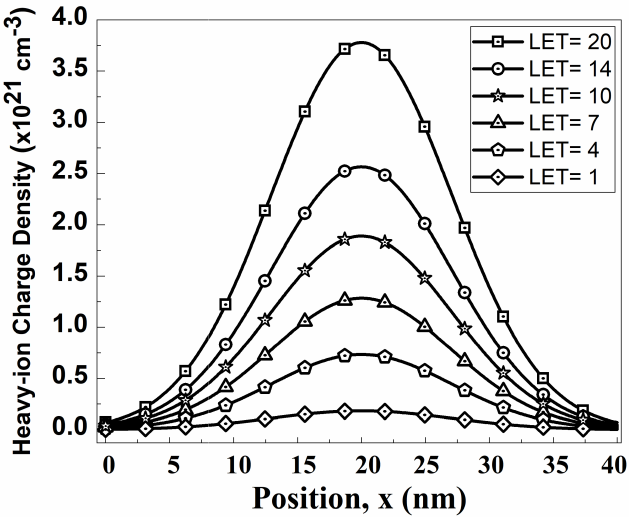

FIGURE 10. The variation in the heavy-ion charge density is shown with respect to position for different LETs.

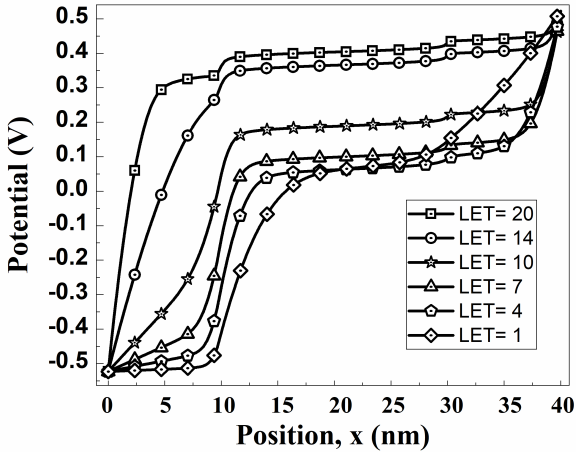

FIGURE 11. Impact of heavy-ion on potential is shown with respect to position for different LET values of heavy-ion.

For LET = 1, 4, and 7 MeV-cm^2/mg the impact is small, which is also observed as the impact of heavy-ions for heavy-ion generation and heavy-ion charge density. For LET = 10 MeV-cm^2/mg, the increase in channel potential is observed as the electron-hole pairs are generating more in this region. However, for LET = 14, and 20 MeV-cm^2/mg the large impact on potential at the source region is observed along with the channel region. This is because, with an increase in LET values, the heavy-ion generation rate expands towards the source, which eventually increases the heavy-ion charge density in the source region as compared to the lower LET values. Although heavy-ion charge density in the source is still low as compared to the channel, which causes the shift of the depletion region towards the source region, and this increases the potential in the source region along with the channel region.

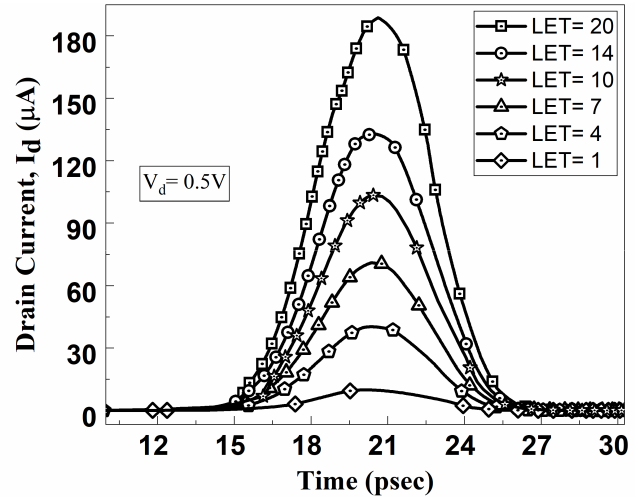

FIGURE 12. The variation in the transient drain current is shown for different LETs with respect to time at 0.5 V drain voltage.

Figure 12 shows the pulses of transient currents for various LETs. The analysis is done for 0.5V drain voltage (Vd) and zero gate-to-source voltage (Vgs). The device with this biasing works in the OFF-state. The observed spike in the drain current is for around 12ps and the peak is achieved at 20 ps. The maximum SET current for all LET values is shown in Fig. 13. For the lowest LET = 1 MeV-cm^2/mg, the maximum transient current achieved is 9.89 μA. For the higher value of LETs; 4, 7, 10, 14 and 20, the maximum transient current achieved are approximately 40 μA, 70 μA, 103 μA, 133 μA and 188 μA. The variation in the transient is due to the collected charge in the device after ion-strikes, higher the LET value, higher the transient current.

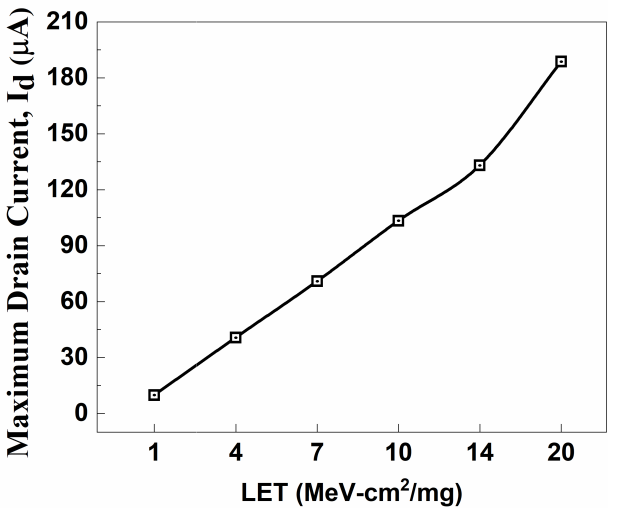

FIGURE 13. Maximum transient drain current is shown for different LETs.

Different SET currents are achieved for different LET and, through that, the charge is collected in the device after ion strikes. It is shown in (8) and the plotted graph is shown in Fig. 14 for different LET values.

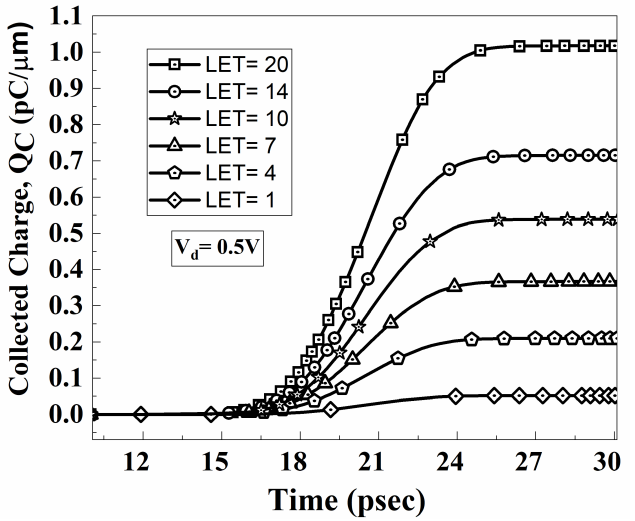

FIGURE 14. The collected charge in the device is shown for different LETs with respect to time.

The collected charge in the device depends on the amount of linear energy transferred in the device radially through the strike of ion. By the graph of Fig. 14, the collected charge can be divided into two regions: exponential and saturation. The higher the energy dropped in the device by an ion, the higher the saturation value of the collected charge in the device. The comparison of a few observed parameters for different LETs has been shown in Table 2. It can be concluded that the collected charge in the device approximately doubles as the heavy-ions energy doubles. The same pattern is observed for heavy-ion charge density and the transient drain current.

TABLE 2. Heavy-ion charge density, maximum transient current, and collected charge are reported for different linear energy transfer values.

LET (MeV-cm^2/mg)	Heavy-Ion charge density (x10^{21} cm^{-3})	Maximum Transient Current (μA)	Deposited Charge (pC/μm)	Collected Charge (pC/μm)
1	0.183	9.89	0.0103	0.052
4	0.73	40	0.041	0.208
7	1.28	70	0.07	0.366
10	1.88	103	0.103	0.538
14	2.56	133	0.14	0.715
20	3.78	188	0.206	1.017

Another parameter that is calculated to analyze the impact of heavy-ion is bipolar gain (β). It is the amplification of charge deposited in the device when a heavy-ion strikes. It is defined as the ratio of collected charge (Q_C) and the deposited charge (Q_d) associated with heavy-ion [28], [29], [30].

$$\beta = Q_d/Q_d \tag{10}$$

The mechanism behind bipolar gain can be demonstrated when a heavy-ion strikes the device, creating electron-hole

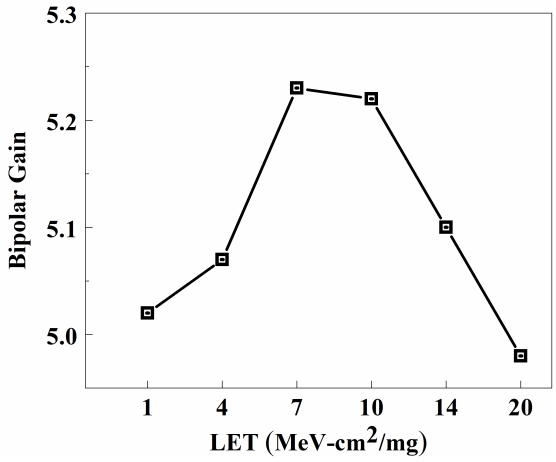

FIGURE 15. Bipolar-gain is shown for different LETs when heavy-ion strikes at body region.

pairs. In the generated electron-hole pairs, the majority of carriers' lifetimes are long, which is also responsible for the rise in potential. Due to the generated electron-hole pairs, transient currents amplify, and so do the charges collected in the device. The collected charge and the deposited charge for different LETs are shown in Table 2, and the bipolar gain graph is shown in Fig. 15 for different LETs. The observed value of bipolar gain is greater than 1, which refers to the effective impact of heavy-ion radiation on DUT, and due to this, errors in the system output may occur.

IV. CONCLUSION

The impact of heavy-ions on DG-TFET is successfully analyzed by striking the heavy-ions vertically at 5 different locations, and the body region is found to be the most sensitive among them. So, the analysis is done for the body region by transient simulations at different LETs. With the strike of heavy-ion, the logic state of the device changes, and it shifts to an ON-state from an OFF-state. The radial generation rate is an important factor for heavy-ions, and in this study, the heavy-ion generation rate and charge density are observed by considering it in the heavy-ion model. Further, the transient current is successfully observed in this study for heavy-ions having LET values of 1, 4, 7, 10, 14, and 20 MeV-cm^2/mg. Later, with the help of the collected charge, the charge that could be collected in the device for different energy heavy-ions is calculated effectively and is found to be higher than the deposited charge. It is found that the transient current is much higher than the ON-current of the device, which shows the possibility of switching of logic state from OFF-to ON-state. The observed value of bipolar gain is greater than 1, which suggests the high impact of radiation on DUT which can damage the device and also introduce errors in the system output.

REFERENCES

[1] A. Seabaugh and Q. Zhang, "Low-voltage tunnel transistors for beyond CMOS logic," *Proc. IEEE*, vol. 98, no. 12, pp. 2095–2110, Oct. 2010, doi: 10.1109/JPROC.2010.2070470.

[2] X. Wang, Z. Tang, L. Cao, J. Li, and Y. Liu, "Gate field plate structure for subthreshold swing improvement of Si line-tunneling FETs," *IEEE Access*, vol. 7, pp. 100675–100683, 2019, doi: 10.1109/ACCESS.2019.2928692.

[3] A. M. Ionescu and H. Riel, "Tunnel field-effect transistors as energy-efficient electronic switches," *Nature*, vol. 479, no. 7373, pp. 37–329, 2011, doi: 10.1038/nature10679.

[4] W. M. Reddick and G. A. J. Amaratunga, "Silicon surface tunnel transistor," *Appl. Phys. Lett.*, vol. 67, no. 4, pp. 494–496, Jul. 1995, doi: 10.1063/1.114547.

[5] S. Datta, H. Liu, and V. Narayanan, "Tunnel FET technology: A reliability perspective," *Microelectron. Rel.*, vol. 54, no. 5, pp. 861–874, May 2014, doi: 10.1016/j.microrel.2014.02.002.

[6] K. Boucart and A. M. Ionescu, "Double-gate tunnel FET with high-K gate dielectric," *IEEE Trans. Electron Devices*, vol. 54, pp. 1725–1733, Jul. 2007, doi: 10.1109/TED.2007.899389.

[7] P.-F. Wang, K. Hilsenbeck, T. Nirschl, M. Oswald, C. Stepper, M. Weis, D. Schmitt-Landsiedel, and W. Hansch, "Complementary tunneling transistor for low power application," *Solid-State Electron.*, vol. 48, no. 12, pp. 2281–2286, Dec. 2004, doi: 10.1016/j.sse.2004.04.006.

[8] A. Dubey, R. Narang, M. Saxena, and M. Gupta, "Investigation of total ionizing dose effect on SOI tunnel FET," *Superlattices Microstruct.*, vol. 133, Sep. 2019, Art. no. 106186, doi: 10.1016/j.spmi.2019.106186.

[9] J. L. Shinn, F. A. Cucinotta, J. W. Wilson, G. D. Badhwar, P. M. O'Neill, and F. F. Badavi, "Effects of target fragmentation on evaluation of LET spectra from space radiation in low-Earth orbit (LEG) environment: Impact on SEU predictions," *IEEE Trans. Nucl. Sci.*, vol. 42, no. 6, pp. 2017–2025, Dec. 1995, doi: 10.1109/23.489248.

[10] G. D. Badhwar and P. M. O'Neill, "Improved model of galactic cosmic radiation for space exploration emission," *Int. J. Radiat. Appl. Instrum. D, Nucl. Tracks Radiat. Meas.*, vol. 20, no. 3, pp. 403–410, 1992, doi: 10.1016/1359-0189(92)90024-P.

[11] *Sentaurus User's Manual*, Synopsys, Inc., Mountain View, CA, USA, 2012.

[12] K. Castellani-Coulie, D. Munteanu, V. Ferlet-Cavrois, and J. Autran, "Simulation analysis of the bipolar amplification in fully-depleted SOI technologies under heavy-ion irradiations," *IEEE Trans. Nucl. Sci.*, vol. 52, no. 5, pp. 1474–1479, Oct. 2005, doi: 10.1109/TNS.2005.855810.

[13] F. A. Ikraiam, "An analysis of radiation effects on electronics and SOI-MOS devices as an alternative," in *Proc. Int. Conf. Sustain. Develop. Through Nucl. Res. Educ.*, vol. 47, no. 1, 2013, pp. 6–14.

[14] T. Colladant, O. Flament, A. L'Hoir, V. Ferlet-Cavrois, C. D'Hose, and J. du P. de Potcharra, "Study of transient current induced by heavy-ion in NMOS/SOI transistors," *IEEE Trans. Nucl. Sci.*, vol. 49, no. 6, pp. 2957–2964, Dec. 2002, doi: 10.1109/TNS.2002.805437.

[15] Q. Wang, H. Liu, S. Wang, and S. Chen, "TCAD simulation of single-event-transient effects in L-shaped channel tunneling field-effect transistors," *IEEE Trans. Nucl. Sci.*, vol. 65, no. 8, pp. 2250–2259, Aug. 2018, doi: 10.1109/TNS.2018.2851366.

[16] Y. Wang, X.-W. He, and C. Shan, "A simulation study of SoI-like bulk silicon MOSFET with improved performance," *IEEE Trans. Electron Devices*, vol. 61, no. 9, pp. 3339–3344, Sep. 2014, doi: 10.1109/TED.2014.2340406.

[17] G. Kaushal, S. S. Rathod, S. Maheshwaram, S. K. Manhas, A. K. Saxena, and S. Dasgupta, "Radiation effects in Si-NW GAA FET and CMOS inverter: A TCAD simulation study," *IEEE Trans. Electron Devices*, vol. 59, no. 5, pp. 1563–1566, May 2012, doi: 10.1109/TED.2012.2187656.

[18] P. Huang, S. Chen, J. Chen, B. Liang, and Y. Chi, "Heavy-ion-induced charge sharing measurement with a novel uniform vertical inverter chains (UniVIC) SEMT test structure," *IEEE Trans. Nucl. Sci.*, vol. 62, no. 6, pp. 3330–3338, Dec. 2015, doi: 10.1109/TNS.2015.2486774.

[19] M. Raine, G. Hubert, P. Paillet, M. Gaillardin, and A. Bournel, "Implementing realistic heavy ion tracks in a SEE prediction tool: Comparison between different approaches," in *Proc. 12th Eur. Conf. Radiat. Effects Compon. Syst.*, Sep. 2011, pp. 363–370, doi: 10.1109/RADECS.2011.6131346.

[20] M. Raine, A. Valentin, M. Gaillardin, and P. Paillet, "Improved simulation of ion track structures using new Geant4 models—Impact on the modeling of advanced technologies response," *IEEE Trans. Nucl. Sci.*, vol. 59, no. 6, pp. 2697–2703, Dec. 2012, doi: 10.1109/TNS.2012.2220783.

[21] M. Murat, A. Akkerman, and J. Barak, "Electron and ion tracks in silicon: Spatial and temporal evolution," *IEEE Trans. Nucl. Sci.*, vol. 55, no. 6, pp. 3046–3054, Dec. 2008, doi: 10.1109/TNS.2008.2007646.

[22] Q. Huang, R. Huang, Z. Zhan, Y. Qiu, W. Jiang, C. Wu, and Y. Wang, "A novel Si tunnel FET with 36 mV/dec subthreshold slope based on junction depleted-modulation through striped gate configuration," in *IEDM Tech. Dig.*, Dec. 2012, pp. 8.5.1–8.5.4, doi: 10.1109/IEDM.2012.6479005.
[23] C. Sandow, J. Knoch, C. Urban, and S. Mantl, "Improving the performance of band-to-band tunneling transistors by tuning the gate oxide and the dopant concentration," in *Proc. Device Res. Conf.*, Jun. 2008, pp. 79–80, doi: 10.1109/DRC.2008.4800743.
[24] R. Sithanandam and M. J. Kumar, "A new on-chip ESD strategy using TFETs-TCAD based device and network simulations," *IEEE J. Electron Devices Soc.*, vol. 6, pp. 298–308, 2018, doi: 10.1109/JEDS.2018.2797054.
[25] S. Saha, "MOSFET test structures for two-dimensional device simulation," *Solid-State Electron.*, vol. 38, no. 1, pp. 69–73, Jan. 1995, doi: 10.1016/0038-1101(94)E0050-O.
[26] G. Tian, J. Bi, G. Xu, K. Xi, X. Yang, H. Yin, Q. Xu, and W. Wang, "Heavy ion induced single-event-transient effects in nanoscale ferroelectric vertical tunneling transistors by TCAD simulation," *Semicond. Sci. Technol.*, vol. 35, no. 10, Oct. 2020, Art. no. 105010, doi: 10.1088/1361-6641/aba549.
[27] Y. Wu and Y. Takahash, "The impact of tunnel FET on heavy ion induced transient effect," in *Proc. ECS Meeting*. Chesapeake, VA, USA, Oct. 2017, doi: 10.1149/MA2017-02/26/1143.
[28] D. Munteanu and J. L. Autran, "Modeling and simulation of single-event effects in digital devices and ICs," *IEEE Trans. Nucl. Sci.*, vol. 55, no. 4, pp. 1854–1878, Aug. 2008, doi: 10.1109/TNS.2008.2000957.
[29] J. J. Quinn, G. Kawamoto, and B. D. McCombe, "Subband spectroscopy by surface channel tunneling," *Surf. Sci.*, vol. 73, pp. 190–196, May 1978, doi: 10.1016/0039-6028(78)90489-2
[30] C. Cai, Z. He, T. Liu, G. Chen, J. Yu, L. Xu, and J. Liu, "Characterization of heavy ion induced SET features in 22-nm FD-SOI testing circuits," *IEEE Access*, vol. 8, pp. 45378–45389, 2020, doi: 10.1109/ACCESS.2020.2978201.
[31] D. Munteanu and J. L. Autran, "3D simulation of single-event-transient effects in symmetrical dual-material double-gate MOSFETs," *Microelectron. Rel.*, vol. 55, nos. 9–10, pp. 1522–1526, Aug. 2015, doi: 10.1016/j.microrel.2015.07.022.
[32] Y. Sun, J. Shao, Z. Liu, X. Li, Y. Liu, and Y. Shi, "Evaluation of single-event-transient effects in reconfigurable field effect transistor beyond 3 nm technology node," *IEEE Trans. Electron Devices*, vol. 68, no. 12, pp. 6001–6006, Dec. 2021, doi: 10.1109/TED.2021.3119006.
[33] B. Ye, L.-H. Mo, P.-F. Zhai, L. Cai, T. Liu, Y.-N. Yin, Y.-M. Sun, and J. Liu, "Impact of heavy ion energy and species on single-event upset in commercial floating gate cells," *Microelectron. Rel.*, vol. 120, May 2021, Art. no. 114128, doi: 10.1016/j.microrel.2021.114128.
[34] M. Raine, "Impact of the radial ionization profile on SEE prediction for SOI transistors and SRAMs beyond the 32-nm technological node," *IEEE Trans. Nucl. Sci.*, vol. 58, no. 3, pp. 840–847, Jun. 2011, doi: 10.1109/TNS.2011.2109966.
[35] H. Liu, M. Cotter, S. Datta, and V. Narayanan, "Soft-error performance evaluation on emerging low power devices," *IEEE Trans. Device Mater. Rel.*, vol. 14, no. 2, pp. 732–741, Jun. 2014, doi: 10.1109/TDMR.2014.2316505.
[36] M. Sharma, R. Narang, M. Saxena, and M. Gupta, "Single event transient effect on tapered angle hetero-junction dopingless TFET for radiation sensitive applications," in *Proc. IEEE VLSI Device Circuit Syst. (VLSI DCS)*, Feb. 2022, pp. 261–264, doi: 10.1109/VLSIDCS53788.2022.9811459.

ASHISH MAURYA received the master's degree from the Indian Institute of Information Technology and Management Gwalior, India, in 2017. He is currently pursuing the Ph.D. degree with the Department of Electronics Engineering, IIT (ISM) Dhanbad, Dhanbad, India. His current research interests include semiconductor physics, nanoelectronics, and emerging semiconductor materials.

KALYAN KOLEY (Senior Member, IEEE) received the master's degree from the National Institute of Technology, Silchar, India, in 2009, and the Ph.D. degree from the Department of Electronics and Telecommunication Engineering, Jadavpur University, Kolkata, India, in 2015. He was a DST-INSPIRE Faculty Member with the Department of Electronics Engineering, IIT (ISM) Dhanbad, Dhanbad, India. He is currently an Assistant Professor with BIT Mesra, Ranchi, Jharkhand, India. His current research interests include the simulation of multiple gate MOSFETs and device modeling of MOSFETs.

JITENDRA KUMAR (Senior Member, IEEE) received the master's degree from IIT Kanpur, Kanpur, India, and the Ph.D. degree from Rajiv Gandhi Technical University, Bhopal, India. He is currently a Professor with the Department of Electronics Engineering, IIT (ISM) Dhanbad, Dhanbad, India. His current research interests include semiconductor physics, nanophotonics, and nanoelectronics.

PANKAJ KUMAR (Graduate Student Member, IEEE) received the master's degree from the National Institute of Technology, Silchar, India, in 2017. He is currently pursuing the Ph.D. degree with the Department of Electronics Engineering, IIT (ISM) Dhanbad, Dhanbad, India. His current research interests include semiconductor physics, nanoelectronics, and emerging semiconductor materials.